Arch. Metall. Mater. **71** (2026), 2, 647-652

DOI: https://doi.org/10.24425/amm.2026.158857

QINGHUA MENG[1*], NING CAO[1]

MICROSTRUCTURAL ANALYSIS OF CORROSION MECHANISMS IN ROTARY RINGS OF CALCINING FURNACES USED IN SODA ASH PRODUCTION

Severe surface corrosion of riding rings in rotary steam calcining furnaces commonly occurs during soda ash production, threatening operational stability and increasing maintenance costs. In this study, forged 35CrMo steel riding rings were investigated to clarify their corrosion behaviour and mechanisms. Environmental media analysis combined with hardness testing, metallographic observation, chemical composition analysis, and SEM-EDS characterisation was employed to examine microstructural evolution, corrosion morphology, and mechanical degradation. The results demonstrate that the corrosion is governed by the synergistic action of electrochemical corrosion in an alkaline dust environment, hydraulic shock caused by lubricant entrapment, and alternating compressive stresses during operation. Pronounced iron oxide formation, severe surface damage, and significant hardness reduction were observed in corroded regions. This study elucidates the coupled corrosion mechanisms of riding rings and provides guidance for lubrication optimisation and service life extension of critical components.

Keywords: Soda ash; calcination furnace; roller ring; 35CrMo; corrosion

1. Introduction

In the production of soda ash – whether by the ammonia-soda process, the combined soda process, or natural soda extraction – the calcination step for dehydrating wet sodium bicarbonate is a critical stage [1-2]. The calciner is one of the most essential units in soda ash manufacturing, and as a rotating apparatus, it is characterised by substantial dimensions [3-5]. For example, a commonly used model with a diameter of 3.6 meters has a total furnace length of 40 meters. During regular operation, the combined weight of the equipment, process materials, and condensed steam exceeds 400 metric tons. In 1980, Japan first proposed the dual Solvay process, also known as the modified Solvay process. Although the dual process provided an environmentally friendly route for sodium carbonate production with lower emissions, it ultimately lost economic competitiveness, leading to a decline in its industrial application [6-9]. These furnaces exhibited drawbacks such as low thermal efficiency, limited production capacity, short equipment lifespan, and high maintenance demands. From the late 1960s to the early 1970s, the fluidised-bed steam calcining furnace emerged as a new calcination technology [10-12]. However, its operational cycle was shorter, and its energy consumption slightly higher than that of the rotary steam calcining furnace [13]. During operation, the calcining furnace is fully supported by the front and rear roller rings and the four supporting rollers, rotating under conditions of low speed and heavy load. Coupled with high furnace-body temperatures, excessive alkali dust, and inadequate lubrication, nearly all roller rings in soda ash plants have experienced various forms of corrosion. Once corrosion occurs, repair becomes extremely difficult. Traditional methods, such as welding or machining, cannot eliminate the defects; instead, they tend to accelerate their deterioration. As a result, replacing the roller rings has become the most common solution in later stages [14-17]. However, this approach involves long construction periods and high costs. Observations and analyses indicate that the lubrication method of the roller rings has a significant influence on their corrosion behaviour, a point that will be discussed further in this paper. Therefore, research on the corrosion of roller rings in calcining furnaces is essential [18-20].

2. Experimental procedures

The rolling ring of the calcining furnace is typically made of 35CrMo alloy steel and is produced through integral

[1] INTELLIGENT MANUFACTURING COLLEGE, WEIFANG INSTITUTE OF TECHNOLOGY, CHINA

* Corresponding author: lygjcmqh@163.com

forging. As an alloy structural steel compliant with the GB/T 3077-2015 standard, it possesses high static strength, impact toughness, and fatigue resistance, making it particularly suitable for manufacturing critical components such as rolling rings that are subjected to impact, bending, torsion, and heavy loads. After heat treatment, the hardness of the working surface ranges from HB 170 to 217.

The other mechanical properties are listed in TABLE 1.

TABLE 1

Mechanical Properties of 35CrMo Steel

Tensile strength	Yield point	Elongation rate	Shrinkage rate	Impact toughness	Surface hardness depth
100	85	12	50	8	50

In the field of metallic materials science, 35CrMo steel is known to exhibit poor weldability, primarily due to its high carbon equivalent (Ceq) value of 0.72%. After welding, the material shows a strong tendency toward hardening, which increases the likelihood of hot cracking and cold cracking in the base metal. Therefore, when pitting corrosion develops on the calciner riding ring, repair welding is not recommended.

The service life of a calciner riding ring is directly influenced by its operating environment. The key operational factors, ranked by their degree of impact, are as follows: (1) Lubrication method – commonly used domestic lubricants include liquid lubricating oil, grease, and graphite. (2) Adhesion and penetration of alkaline dust into corrosion pits on the riding ring. (3) Heat transfer from the calciner to the riding ring. (4) Periodic compressive loading during operation. (5) Installation defects leading to slippage of the inner raceway.

Based on the characteristics of the specimens, the following experimental methods were employed: (1) Macroscopic examination of the specimens, with an emphasis on post-corrosion morphology. (2) Material composition analysis of the corroded regions using a fixed direct-reading spectrometer (Thermo Niton XL2, USA). (3) Hardness testing of the corroded areas on the riding ring surface. (4) Comparative metallographic analysis of both corroded and non-corroded regions using a metallurgical microscope (Axio Vert.A1, ZEISS, Germany). (5) Scanning electron microscopy (SEM, ZEISS Sigma 300, Germany) to analyse the micromorphology of the corroded surfaces and further characterise corrosion features. Additionally, energy-dispersive X-ray spectroscopy (EDS, accelerating voltage: 15 kV, working distance: 8.5 mm, and beam current: 10 nA) was performed on the corrosion products to determine their elemental composition and concentrations.

3. Results and discussion

The surface corrosion of the rollers mainly occurs in the areas in contact with the supporting rollers. Therefore, the sampling areas of this study mainly cover these parts. The specific samples are shown in Fig. 1(a), where 1-5 are the monitoring points. The severely corroded rollers are shown in Fig. 1(b).

After corrosion occurs on the rolling ring, numerous pits develop on its surface, indicating severe localised material degradation. The most enormous pits reach depths of approximately 10 mm and cover areas exceeding 100 mm × 100 mm, while in extreme cases, pit diameters exceed 200 mm with depths significantly greater than 10 mm. More than 60% of the rolling-ring surface exhibits severe corrosion damage. Such extensive pitting not only reduces the effective load-bearing area of the rolling ring but also introduces pronounced surface irregularities. When the corroded rolling ring comes into contact with the idler wheel, these pits act as stress concentrators, leading to intensified local contact stress and accelerated wear of both the rolling ring and the idler wheel. This observation highlights that surface corrosion directly contributes to mechanical degradation and secondary component damage under service conditions.

According to available data, the implementation standard for 35CrMo alloy structural steel is GB/T 3077-2015, corresponding to the Japanese standard JIS G4053:2003. The standard specifies the chemical composition of this steel as follows.

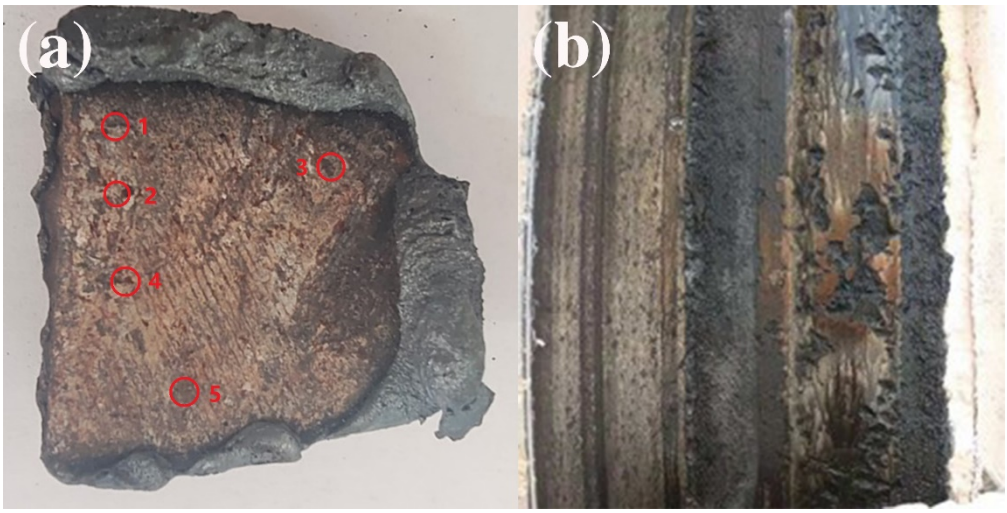

Fig. 1. (a) Rolling ring sampling piece, (b) Surface of the rolling ring after corrosion

TABLE 2

Chemical Composition of 35CrMo Steel

C	Si	Mn	S	P	Cr	Ni	Cu	Mo
0.32~0.40	0.17~0.37	0.40~0.70	≤0.035	≤0.035	0.80~1.10	≤0.030	≤0.030	0.15~0.25

After testing the sample, the measured elemental contents were generally within the specified range, with the iron content being approximately 97.05%.

The rolling rings of the calcining furnace are manufactured from 35CrMo, an excellent alloy structural steel known for its high strength, toughness, and wear resistance. It is well-suited for service conditions involving heavy loads and alternating impacts. During the manufacturing process, quenching and tempering are performed to ensure that the surface hardness of the rolling ring reaches HB 170-217, with a hardened layer thickness exceeding 50 mm.

Before quenching and tempering, 35CrMo primarily consists of a ferrite-pearlite microstructure. After quenching and tempering, the surface microstructure of the rolling ring should transform into a uniform tempered sorbite.

Figs. 2(a-d) show the metallographic images of the sampled specimens under 100× and 20× magnifications.

From the metallographic images, the uncorroded regions of the rolling ring exhibit a relatively uniform microstructure, primarily consisting of tempered sorbite, accompanied by feather-like bainite and a small amount of ferrite precipitated along the grain boundaries. The presence of bainite and grain-boundary ferrite introduces microstructural heterogeneity, which is known to increase the susceptibility of Cr–Mo alloy steels to localised corrosion and stress-assisted damage. In the corroded regions, surface pits propagate inward along these microstructural features, indicating that microstructural non-uniformity plays an important role in corrosion initiation and growth. Under cyclic compressive loading during furnace operation, these localised defects further intensify stress concentration, thereby accelerating material degradation. Previous studies have shown that tempered sorbite and bainitic structures in Cr–Mo alloy steels exhibit distinct corrosion sensitivities and degradation behaviours under service environments, particularly when grain-boundary ferrite is present [21]. In the metallographic image of the sample edge at 20× magnification (Fig. 2(d)), the bright area corresponds to the uncorroded rolling ring material, the brown-black area represents the resin used for metallographic preparation, and the interface between the two indicates the corroded region. At the microscopic scale, surface pits are present and extend inward.

Observations under the scanning electron microscope (SEM) reveal that the surface of the corroded rolling ring is severely fractured, with the material integrity disrupted. The surface exhibits a hill-like morphology with clear erosion marks. Localised surface protrusions are evident, some of which have begun to delaminate. The edges of the resulting gaps are gradually smoothing and enlarging, with the gaps continuing to propagate inward into the material. Figs. 3(a-d) show the SEM images of the sample analysed in this study.

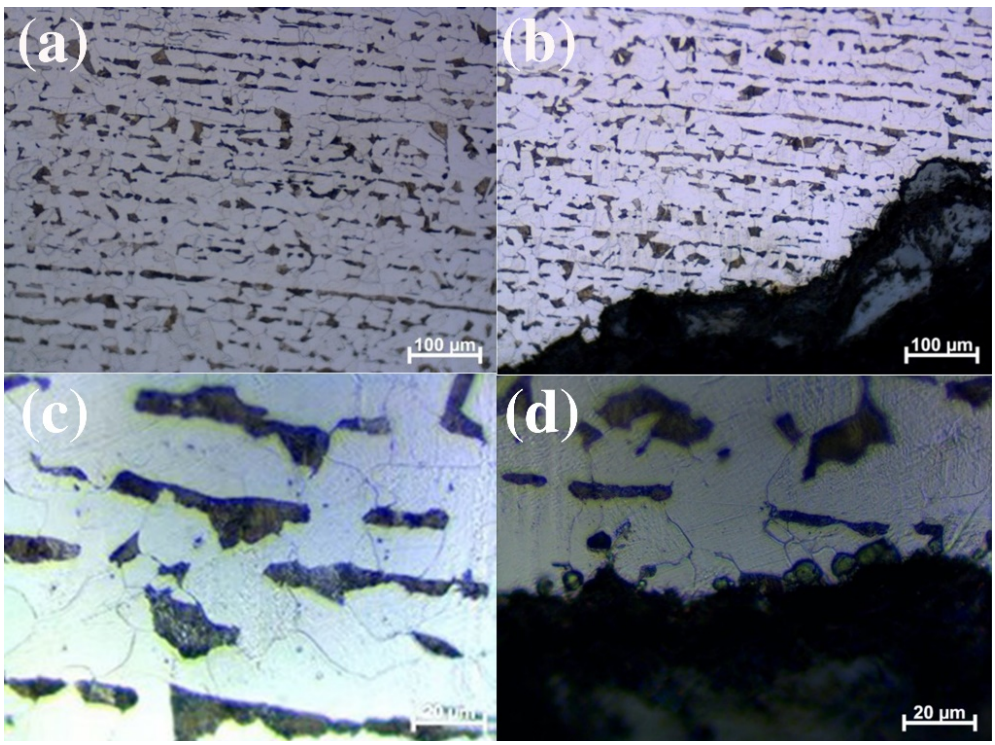

Fig. 2. (a) Metallographic image of the sample at 100 µm magnification; (b) Metallographic image of the sample's critical edge at 100 µm magnification; (c) Metallographic image of the sample at 20 µm magnification; (d) Metallographic image of the sample's edge at 20 µm magnification

TABLE 3

Overall Graph of Element Contents

Line spectrum diagram					
Element	**Signal Type**	**Line**	**Wt.%**	**Wt.% Sigma**	**At.%**
C	EDS	K-line system	8.18	0.08	19.02
O	EDS	K-line system	27.13	0.05	47.38
Al	EDS	K-line system	0.06	0.01	0.06
Si	EDS	K-line system	0.05	0.01	0.05
P	EDS	K-line system	0.01	0.01	0.01
S	EDS	K-line system	0.05	0.01	0.05
Cl	EDS	K-line system	3.96	0.01	3.12
Ti	EDS	K-line system	0.00	0.01	0.00
Cr	EDS	K-line system	0.03	0.01	0.02
Mn	EDS	K-line system	0.28	0.02	0.14
Fe	EDS	K-line system	60.19	0.07	30.12
Ni	EDS	K-line system	0.06	0.03	0.03

Based on the above data, EDS analysis was performed to determine the main elemental composition in the selected line-scan area. The results clearly indicate changes in the total content of each element, with Fe and O showing the most significant variations. According to the standard, the Fe content of 35CrMo steel is approximately 97.05%, while the O content is not specified, but it is expected to be lower than that of other trace elements. In the present analysis, the Fe content decreases to 60.19%. In comparison, the O content increases to 27.13%, confirming the formation of a substantial amount of iron oxides within the corrosion layer of the surface pits. This compositional change indicates that oxidation-dominated electrochemical corrosion is a significant degradation mechanism affecting the rolling ring surface. In the alkaline dust-rich environment of the calcining furnace, corrosive species can readily accumulate within surface defects and lubricant-retained regions, promot-

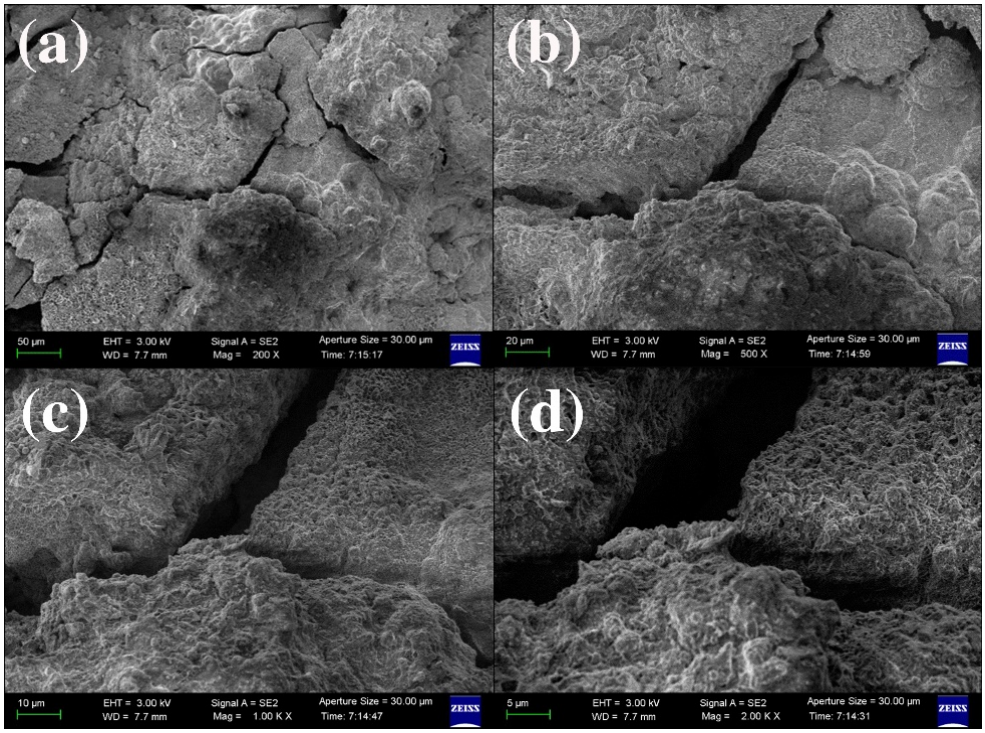

Fig. 3. Scanning electron microscope images (a) 50 μm (b) 20 μm (c) 10 μm (d) 5 μm

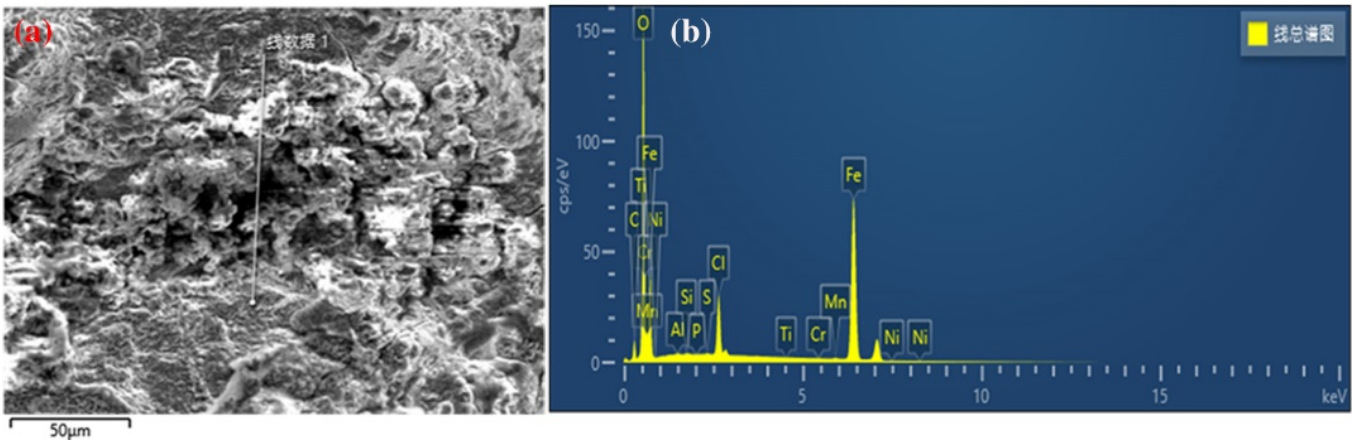

Fig. 4. (a) shows the image of the corroded surface scanned by the rolling ring, (b) presents the chemical composition analysis

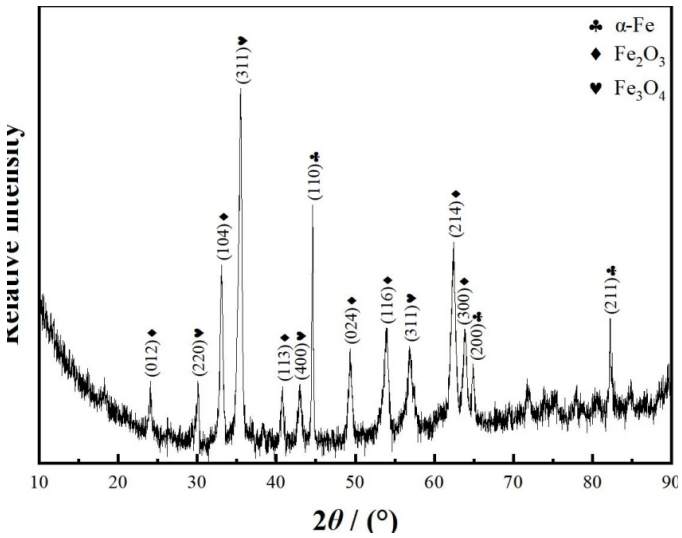

Fig. 5. X-ray diffraction pattern of corrosion products on the riding ring surface, showing the presence of Fe_2O_3, Fe_3O_4, and residual α-Fe

ing localised electrochemical reactions. Moreover, lubricant trapped in corrosion pits may generate hydraulic shock under cyclic compressive loading, further accelerating pit growth and surface material detachment. These combined effects explain the severe localised corrosion observed in service-exposed rolling rings. Similar oxidation-dominated corrosion behaviour of steel materials exposed to alkaline or industrial dust-containing environments has been widely reported in previous environmental and materials studies [22]. These findings are consistent with the previously discussed corrosion mechanism.

To further identify the phase composition of the corrosion products indicated by the EDS results, X-ray diffraction (XRD) analysis was performed on the corroded surface layer. The XRD pattern (Fig. 5) reveals distinct diffraction peaks corresponding to Fe_2O_3 and Fe_3O_4, together with residual α-Fe from the substrate. The presence of Fe_2O_3 indicates dominant oxidative corrosion under alkaline and oxygen-rich service conditions, whereas Fe_3O_4 suggests non-uniform oxygen availability within corrosion pits. These results confirm that the elevated oxygen content detected by EDS originates from iron oxide formation rather than surface contamination, thereby strengthening the proposed oxidation-dominated electrochemical corrosion mechanism.

In metallic materials science, the standard hardness of 35CrMo steel after quenching and tempering is HB ≤ 229. The hardness of the working surface of the calcining furnace rolling ring ranges from HB 170 to 217. Hardness measurements were performed at five points on the sample, and the results are summarized in the table below. The specific test positions are shown in Fig. 1(a). The five test points were deliberately selected within the drum-support contact area, which represents the region with the most severe corrosion and the highest mechanical stress during use. Measurements were taken in representative areas, including the centre of the corrosion pits, the edges of the pits, and the relatively intact areas adjacent to the pits, in order to capture the local degradation caused by corrosion and alternating compressive stress.

TABLE 4

Hardness Test Values

1	2	3	4	5
151.8	134.0	142.3	150.6	159.8

The measured hardness values after corrosion decrease to 134-160 HB, which are significantly lower than the designed surface hardness range of 170-217 HB for the rolling ring. This reduction indicates a pronounced degradation of surface mechanical properties. Once the softened rolling ring surface comes into direct contact with the idler wheels, accelerated wear and surface damage are inevitable, further shortening the service life of both components. Therefore, the observed hardness reduction provides quantitative evidence that corrosion directly compromises the mechanical reliability of the rolling ring under actual operating conditions. Therefore, the corrosion behaviour of the riding ring cannot be attributed to a single factor, but rather to the combined effects of electrochemical reactions, lubricant-induced hydraulic shock, and alternating compressive stresses during service. Similar synergistic corrosion mechanisms involving the coupling of mechanical stress and electrochemical reactions have been reported for metallic components operating under complex service conditions [23].

4. Conclusion

(1) Severe surface corrosion was observed on forged 35CrMo steel rolling rings after long-term service in a rotary steam calcining furnace. More than 60% of the surface area exhibited extensive pitting corrosion, with pit depths exceeding 10 mm in severely damaged regions.

(2) SEM-EDS analysis revealed a significant increase in oxygen content (up to 27.13%) and a corresponding decrease in iron content (to approximately 60.19%) within corrosion pits, confirming that oxidation-dominated electrochemical corrosion is a primary degradation mechanism under alkaline dust-rich industrial environments.

(3) Hardness measurements showed that the surface hardness of the corroded rolling ring decreased to 134-160 HB, falling below the design requirement of 170-217 HB. This reduction quantitatively demonstrates the deterioration of load-bearing capacity induced by corrosion.

(4) The corrosion behaviour of the rolling rings is governed by the synergistic coupling of electrochemical corrosion, lubricant-induced hydraulic shock, and alternating compressive stresses during operation, rather than by a single degradation mechanism.

(5) The findings highlight the critical importance of lubrication optimisation and environmental control in mitigating corrosion damage. This study provides practical guidance for extending the service life of rolling rings and similar heavy-duty load-bearing components in rotary industrial equipment.

REFERENCES

[1] H. Rahimpour, A. Fahmi, S. Zinatloo-Ajabshir, Toward sustainable soda ash production: a critical review on eco-impacts, modifications, and innovative approaches. Results in Engineering **23**, 102399 (2024).
DOI: http://doi.org/10.1016/j.rineng.2024.102399

[2] H.G.D.A. Villardi, L. Yokoyama, A. Young, A.A. Veiga, S. Pagnin, Experimental methodology for CO_2 capture and sodium bicarbonate synthesis with producedwater from oil industry. J. Pet. Explor. Prod. Technol. **12**, 2577-2585 (2022).
DOI: http://doi.org/10.1007/s13202-022-01479-0

[3] J. Wisniak, Sodium carbonate-From natural resources to Leblanc and back. Indian J. Chem. Technol. **10**, 99-112 (2003).
DOI: http://doi.org/10.1016/j.jclepro.2023.136201

[4] H. Chen, X. Chen, W. Tan, P. Wu, Y. Zhang, Durability performance of waste glass powder and calcium oxide added sodium carbonate-activated slag mortar. Mater. Today Commun. **36**, 106472 (2023).
DOI: http://doi.org/10.1016/j.mtcomm.2023.106472

[5] W. Deng, C. Spathi, T. Coulbeck, K. Erhan, D. Backhouse, M. Marshall, R. Ireson, P.A. Bingham, Exploratory research in alternative raw material sources and reformulation for industrial soda-lime-silica glass batches. International Journal of Applied Glass Science **11**, 340-356 (2020).
DOI: http://doi.org/10.1111/ijag.14775

[6] K.M. Wagialla, I. Al-Mutaz, M. El-Dahshan, The manufacture of soda ash in the Arabian Gulf. International Journal of Production Economics **27**, 145-153 (1992).
DOI: http://doi.org/10.1016/0925-5273(92)90007-t

[7] M. Cichosz, U. Kiełkowska, S. Łazarski, Ł. Kiedzik, M. Szkudlarek, K. Skowron, B. Kowalska, D. Żurawski, Influence of ammonia concentration on Solvay soda process parameters and associated environmental and energetic effects. Energies **15**, 8370 (2022). DOI: http://doi.org/10.3390/en15228370

[8] M.V. Meshalkin, N. Shulaev, N. Bykovsky, V. Aristov, Physicochemical foundations of an energy and resource efficient combined technology for processing of soda ash production wastewater. Dokl. Chem. **494** (1), 145-148 (2020).
DOI: http://doi.org/10.1134/s0012500820090025

[9] A.A.I. Mourad, A.F. Mohammad, A.H. Al-Marzouqi, M.H. El-Naas, M.H. Al-Marzouqi, M. Altarawneh, KOH-based modified solvay process for removing na ions from high salinity reject brine at high temperatures. Sustainability-Basel **13**, 10200 (2021).
DOI: http://doi.org/10.3390/su131810200

[10] A.-H.M. Aya, A.F. Mohammad, A.H. Al-Marzouqi, M.H. El-Naas, M.H. Al-Marzouqi, M. Altarawneh, CO_2 capture and ions removal through reaction with potassium hydroxide in desalination reject brine: Statistical optimization. Chem Eng Process **170**, 108722 (2022).
DOI: http://doi.org/10.1016/j.cep.2021.108722

[11] D. Wysocki, A. Szymanek, The effectiveness of modified sodium bicarbonate in the purification of exhaust gases from HCl and HF. Journal of Achievements in Materials and Manufacturing Engineering **114**, 57-66 (2022).
DOI: http://doi.org/10.5604/01.3001.0016.2156

[12] I.-H. Hwang, T. Matsuo, T. Matsuto, Y. Tojo, R. Sameshima, Dry scrubbing of municipal solid waste incineration flue gas using porous sodium carbonate produced via vacuum thermal treatment of sodium bicarbonate. J. Mater. Cycles Waste Manage. **23**, 1609-1616 (2021).
DOI: http://doi.org/10.1007/s10163-021-01241-4

[13] X. Wang, G. Wang, L. Zhang, Green and simple production of graphite intercalation compound used sodium bicarbonate as intercalation agent. BMC Chem. **16**, 13 (2022).
DOI: http://doi.org/10.1186/s13065-022-00808-y

[14] G. Steinhauser, Cleaner production in the Solvay Process: general strategies and recent developments. J. Cleaner Prod. **16**, 833-841 (2008). DOI: http://doi.org/10.1016/j.jclepro.2007.04.005

[15] L. Bonfim-Rocha, A.B. Silva, S.H.B. de Faria, M.F. Vieira, M. de Souza, Production of sodium bicarbonate from CO_2 reuse processes: A brief review. Int. J. Chem. Reactor Eng. **18**, 20180318 (2020). DOI: http://doi.org/10.1515/ijcre-2018-0318

[16] N.A. Halim, N.Z. Kasim, A.R.M. Radzi, F. Turan, A Proposed Methodological Considerations for Sustainable Chemical Process Design. Key Engineering Materials **938**, 123-131 (2022).
DOI: http://doi.org/10.4028/p-5b44o6

[17] O.V. Kharissova, B.I. Kharisov, C.M. Oliva Gonzalez, Y.P. Méndez, I. López, Greener synthesis of chemical compounds and materials. R. Soc. Open Sci. **6**, 191378 (2019).
DOI: http://doi.org/10.1098/rsos.191378

[18] S. Kushwaha, J. Baranwal, S. Singh, A. Jyoti, A review on green synthesis of biologically active compounds. Current Green Chemistry **9**, 174-195 (2020).
DOI: http://doi.org/10.2174/2213346110666221213092734

[19] T. Setayeshmanesh, M.M. Parivazh, M. Abbasi, S. Osfouri, M.J. Dianat, M. Akrami, Reducing the environmental impacts of desalination reject brine using modified solvay process based on calcium oxide. Sustainability-Basel **14**, 22-98 (2020).
DOI: http://doi.org/10.3390/su14042298

[20] N. Mohammed, P. Palaniandy, F. Shaik, B. Deepanraj, H. Mewada, Statistical analysis by using soft computing methods for seawater biodegradability using ZnO photocatalyst. Environ. Res. **227**, 115696 (2023).
DOI: http://doi.org/10.1016/j.envres.2023.115696

[21] P.D. Ioannou, P. Nica, V. Paun, P. Vizureanu, M. Agop, Wave–particle duality through an extended model of the scale relativity theory. Phys. Scr. **78** (6), 065101(2008).
DOI: http://doi.org/10.1088/0031-8949/78/06/065101

[22] M. Agop, P. Ioannou, P. Nica, C. Radu, A. Alexandru, P. Vizureanu, Fractal characteristics of the solidification process. Mater. Trans. **45** (3), 972-975(2004).
DOI: http://doi.org/10.2320/matertrans.45.972

[23] P. Vizureanu, C. Samoilă, D. Cotfas, Materials Processing Using Solar Energy. Environ. Eng. Manage. J. **8** (2) (2009).
DOI: http://doi.org/10.30638/eemj.2009.043